Crystal-field effects in $Er_3Ru_4Al_{12}$ with a distorted kagome lattice

D. I. Gorbunov,[1] I. Ishii,[2] Y. Kurata,[2] A. V. Andreev,[3] T. Suzuki,[2] S. Zherlitsyn,[1] and J. Wosnitza[1,4]

[1]*Hochfeld-Magnetlabor Dresden (HLD-EMFL) and Würzburg-Dresden Cluster of Excellence ct.qmat,*
Helmholtz-Zentrum Dresden-Rossendorf, 01328 Dresden, Germany
[2]*Department of Quantum Matter, ADSM, Hiroshima University, Higashi-Hiroshima 739-8530, Japan*
[3]*FZU Institute of Physics, Czech Academy of Sciences, Na Slovance 2, 182 21 Prague, Czech Republic*
[4]*Institut für Festkörper- und Materialphysik, TU Dresden, 01062 Dresden, Germany*

We report on the magnetic and elastic properties of $Er_3Ru_4Al_{12}$ in static and pulsed magnetic fields up to 58 T. From the ultrasound results, we obtain evidence for a phase transition at 2 K related to magnetic ordering. Furthermore, in the paramagnetic state, $Er_3Ru_4Al_{12}$ shows pronounced anomalies in the magnetization and elastic moduli as a function of temperature and magnetic field. We explain our findings using a crystal-electric-field (CEF) model that includes quadrupolar interactions and propose a CEF level scheme for this material. However, the CEF effects cannot explain all field-induced anomalies, which indicates that refined models are needed for explaining these.

I. INTRODUCTION

Rare-earth compounds with nonmagnetic elements harbor a wealth of intriguing magnetic properties that result from the interplay between exchange interactions, magnetocrystalline anisotropy, magnetoelastic effects, and multipolar interionic couplings. These interactions can be tuned, e.g., by magnetic field and elemental substitution, to explore the rich phase diagrams of rare-earth-based materials. The exchange interactions and single-ion magnetic anisotropy are usually the dominant terms acting on rare-earth ions [1]. Therefore, knowledge of the exchange couplings and crystal-electric-field (CEF) parameters is necessary for a quantitative understanding of the underlying physics.

Recently, $R_3Ru_4Al_{12}$ (with R a rare-earth element or U) came into focus due to their intriguing electronic properties [2–20]. These materials crystallize in a hexagonal structure of $Gd_3Ru_4Al_{12}$ type (space group $P6_3/mmc$) [21–23]. The R atoms are arranged in a distorted kagome lattice, which leads to competing exchange and anisotropy interactions for some members of this group. The distortion is given by two different equilateral triangles with edges of about 5.1 and 3.7 Å within the same atomic layer. The compounds with $R =$ Nd and Pr are ferromagnets [2–4], whereas those with $R =$ Gd, Tb, Dy, Ho, Yb, and U are antiferromagnets [5–20]. For some $R_3Ru_4Al_{12}$, complex magnetic structures were reported, whereby the crystallographic site of the R element lowers its local symmetry due to magnetic ordering [2,3,7,11]. In applied magnetic field, $R_3Ru_4Al_{12}$ show rotations of magnetic moments and CEF transitions. On the basis of the magnetic and elastic properties of $R_3Ru_4Al_{12}$ with $R =$ Dy, Ho, and U, their CEF level schemes were determined [15,16,20]. Quadrupolar interactions were found to play an important role, leading to a pronounced softening of the transverse elastic modulus C_{44}.

Here, we report on the magnetic and elastic properties of $Er_3Ru_4Al_{12}$. In an earlier study, this material was suggested to be on the verge of magnetic ordering just above 2 K [24]. We observe an excessive hardening of longitudinal and transverse elastic moduli below 2 K, which likely reflects an ordering of the Er magnetic moments. We also detect anomalies due to CEF transitions as a function of temperature and magnetic field. Our CEF analysis, which includes quadrupolar interactions, well reproduces most of the temperature and field dependencies of the magnetization and elastic moduli in the paramagnetic state. For this regime, we determined the CEF scheme of $Er_3Ru_4Al_{12}$.

II. EXPERIMENTAL DETAILS

An $Er_3Ru_4Al_{12}$ single crystal was grown from a quasi-stoichiometric mixture of the pure elements (Er 99.9%, Ru 99.99%, Al 99.999%) with an Al mass excess of 1% in a tri-arc furnace by a modified Czochralski method. Standard x-ray diffraction analysis was performed on a part of the single crystal crushed into a fine powder. The lattice parameters of the hexagonal unit cell are $a = 8.755$ Å and $c = 9.483$ Å. The crystal was oriented using backscattered Laue diffraction for magnetization and ultrasound experiments.

The field and temperature dependencies of the magnetization were measured up to 14 T using a commercial physical property measurement system.

High-field magnetization was measured between 2 and 40 K in pulsed magnetic fields up to 58 T by the induction method using a coaxial pick-up coil system (a detailed description of the magnetometer can be found in Ref. [25]). Absolute values of the magnetization were calibrated using data obtained in static fields.

The field and temperature dependencies of the relative sound-velocity changes were measured using an ultrasound
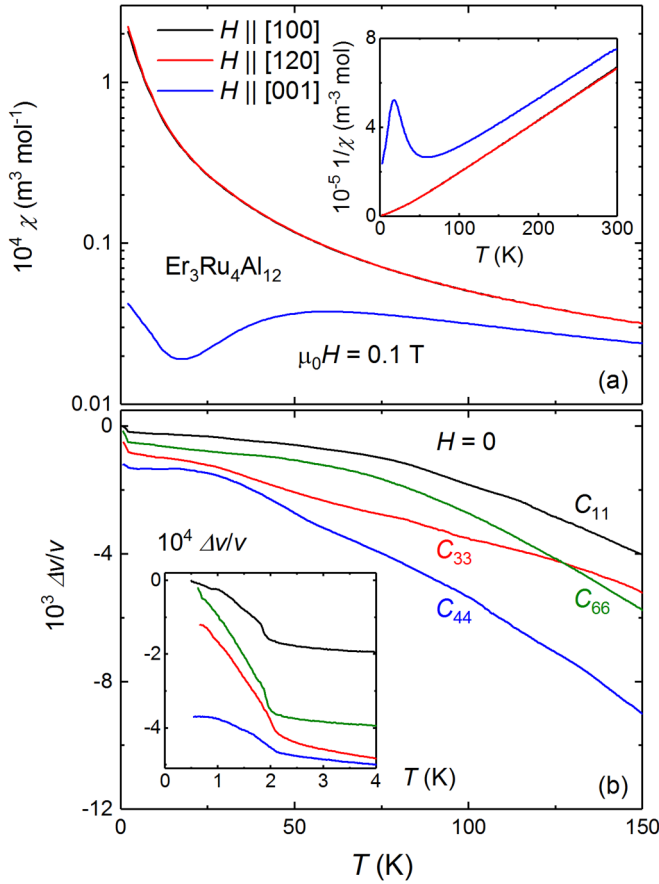
FIG. 1. Temperature dependencies of the (a) magnetic susceptibility, χ, and (b) relative sound velocity, $\Delta v/v$, for various acoustic modes in $Er_3Ru_4Al_{12}$. The inset in panel (a) shows the inverse magnetic susceptibility, $1/\chi$. The inset in panel (b) shows $\Delta v/v$ at low temperatures in enlarged scale. The ultrasound frequencies were 98, 97, 26, and 100 MHz for the acoustic modes C_{11}, C_{33}, C_{44}, and C_{66}, respectively.

pulse-echo phase-sensitive detection technique [26,27]. A pair of piezoelectric transducers were glued to opposite surfaces of the sample to excite and detect acoustic waves. We measured the longitudinal, C_{11} ($k \parallel u \parallel$ [100], where k and u are the wave vector and polarization of acoustic waves, respectively), C_{33} ($k \parallel u \parallel$ [001]), and transverse, C_{44} ($k \parallel$ [100], $u \parallel$ [001]), C_{66} ($k \parallel$ [100], $u \parallel$ [120]) acoustic modes. The absolute values of the sound velocities for these modes at 2 K are $v_{11} = 6057 \pm 50$ m/s, $v_{33} = 6455 \pm 50$ m/s, $v_{44} = 3432 \pm 50$ m/s, and $v_{66} = 3504 \pm 50$ m/s.

III. RESULTS

$Er_3Ru_4Al_{12}$ does not show magnetic ordering above 2 K as can be seen from the magnetic susceptibility, $\chi = M/H$, where M and H are the magnetization and magnetic field, respectively [Fig. 1(a)]. The minimum in χ vs T for $H \parallel$ [001] can be explained by CEF effects (see Sec. IV). At high temperatures, χ follows a Curie-Weiss law [inset in Fig. 1(a)],

$$\chi = \frac{C_0}{T - \theta}, \quad (1)$$

TABLE I. Effective magnetic moments, μ_{eff}, per Er atom and paramagnetic Curie temperatures, θ, for fields applied along the principal crystallographic directions of $Er_3Ru_4Al_{12}$ obtained from fits in the listed temperature ranges.

	$H \parallel$ [100]	$H \parallel$ [120]	$H \parallel$ [001]
μ_{eff} (μ_B/Er)	9.5(1)	9.5(1)	9.6(1)
θ (K)	18(1)	17(1)	−32(1)
Temperature range (K)	100–300	100–300	150–300

where C_0 is the Curie constant proportional to the square of the effective magnetic moment, μ_{eff}, and θ is the Weiss or paramagnetic Curie temperature. As listed in Table I, μ_{eff} is in good agreement with the theoretical value, 9.59 μ_B, for an Er^{3+} ion. The large difference between the θ values for the basal plane and [001] direction, ≈ 50 K, is evidence of a large magnetic anisotropy of $Er_3Ru_4Al_{12}$.

The relative sound velocity, $\Delta v/v$, increases with decreasing temperature [Fig. 1(b)]. Our measurements in a He-3 cryostat reveal additional hardening for all acoustic modes
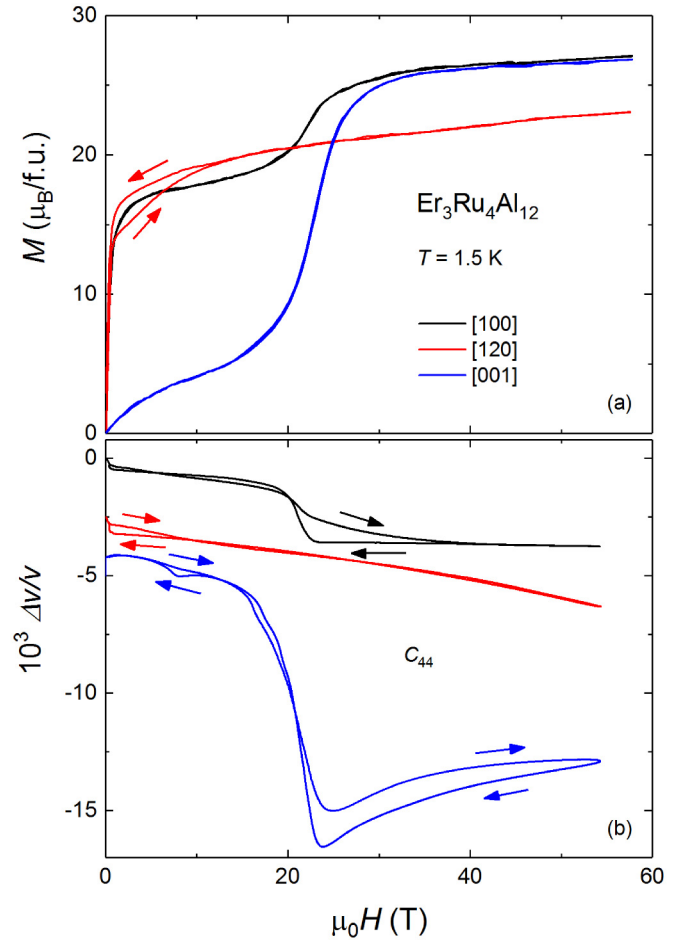

FIG. 2. Field dependencies of the (a) magnetization, M, and (b) relative sound velocity, $\Delta v/v$, for fields applied along the principal crystallographic directions of $Er_3Ru_4Al_{12}$ at 1.5 K. The ultrasound frequencies were 190, 206, and 203 MHz for field applied along the [100], [120], and [001] axes, respectively.
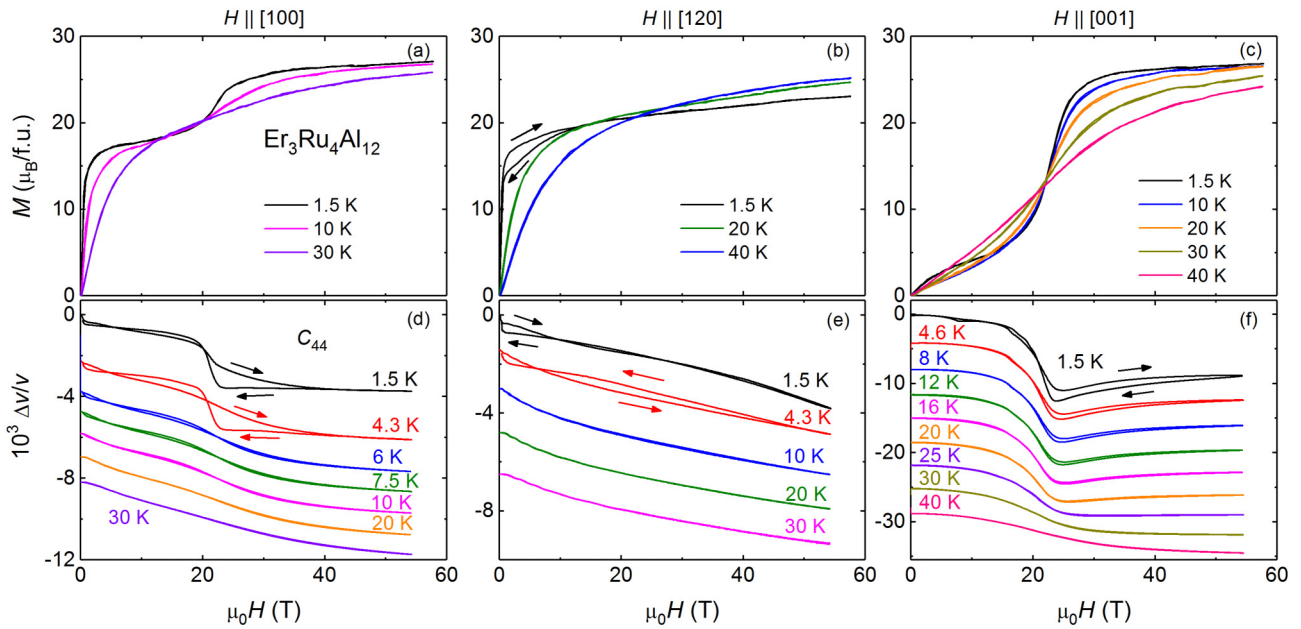
FIG. 3. Field dependencies of the magnetization, M, and relative sound velocity, $\Delta v/v$, for fields applied along the (a), (d) [100]; (b), (e) [120]; and (c), (f) [001] axes of $Er_3Ru_4Al_{12}$ between 1.5 and 40 K. The ultrasound frequencies were 190, 206, and 203 MHz for fields applied along the [100], [120], and [001] axes, respectively.

below 2 K [inset in Fig. 1(b)] due to a phase transition into a magnetically ordered state.

Furthermore, $Er_3Ru_4Al_{12}$ shows anomalies in the magnetization and sound velocity in applied fields. The easy magnetization direction lies in the basal plane, the [001] axis is the hard direction [Fig. 2(a)]. For fields applied along the [100] and [001] axes, $Er_3Ru_4Al_{12}$ exhibits field-induced transitions at about 20 T. For $H \parallel$ [100], the magnetization grows from 20 to 26 μ_B/f.u., whereas, for $H \parallel$ [001], it increases from about 6 to 26 μ_B/f.u. Above the magnetization jumps, the
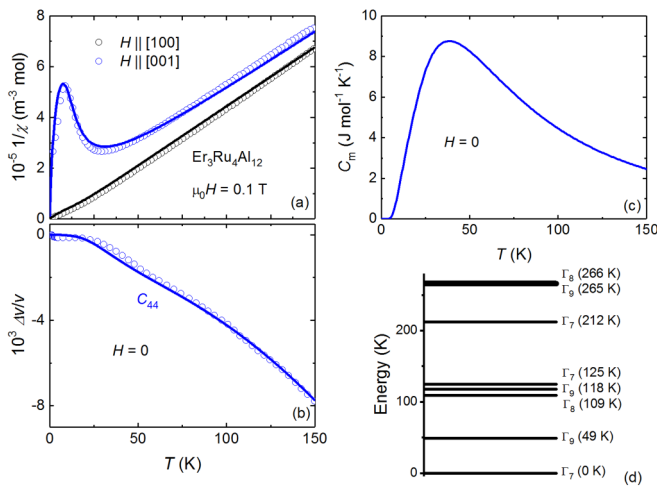

FIG. 4. Temperature dependencies of the (a) inverse magnetic susceptibility, $1/\chi$, (b) relative sound velocity, $\Delta v/v$, and (c) magnetic contribution to the specific heat, C_m, and (d) CEF level scheme of an Er^{3+} ion in $Er_3Ru_4Al_{12}$ obtained from the CEF parameters listed in Table III (see text for details). In panels (a)–(c), the solid lines represent the calculated data. In panels (a) and (b), the symbols represent the experimental data.

full saturation is reached. For this state, the magnetization can be calculated as follows: $M_{sat} = 3 \times M_{Er} = 27 \mu_B$/f.u., where $M_{Er} = 9 \mu_B$ is the magnetic moment per Er^{3+} ion. No anomalies are observed for $H \parallel$ [120] except for a hysteresis below 11 T. For this field direction, the magnetization in the highest field is 23 μ_B/f.u.

As it has been found for the $R_3Ru_4Al_{12}$ compounds with $R =$ Dy [14,15], Ho [16], and U [20], the transverse acoustic mode C_{44} couples to quadrupolar degrees of freedom of these materials. For this reason, we investigated the relative sound velocity for the C_{44} mode of $Er_3Ru_4Al_{12}$ in pulsed magnetic fields [Fig. 2(b)]. $\Delta v/v$ shows a pronounced softening of ≈ 0.002 and ≈ 0.01 at the field-induced anomalies for fields applied along the [100] and [001] axes, respectively. For $H \parallel$ [001], an additional feature is observed at 8 T when the magnetic field is swept down. The origin of this anomaly is not clear. Remarkably, the sound velocity shows a pronounced hysteresis between the field-up and field-down sweeps for fields applied along the [100] and [001] axes, although the magnetization has no hysteresis for these field directions. The origin of the hysteresis might be due to a slower elastic response of the system as compared to the response of the spins to the applied field in this case. Similar to $\Delta v/v$, the magnetization displays hysteresis at low fields for $H \parallel$ [120].

To study the observed features in more detail, we performed magnetization and ultrasound experiments in pulsed magnetic fields at elevated temperatures (Fig. 3). For fields applied along the [100] axis, the anomalies in the magnetization and sound velocity are no longer observed above 10 K [Figs. 3(a) and 3(d)]. For $H \parallel$ [120], the hysteresis in M and $\Delta v/v$ disappears above 4.3 K [Figs. 3(b) and 3(e)]. For $H \parallel$ [001], the transitions can be resolved up to about 30 K [Figs. 3(c) and 3(f)]. The critical fields of the field-induced transitions are temperature independent, which hints

TABLE II. Wave functions, $|J, J_z\rangle$ ($J = 15/2$), of all CEF states for $Er_3Ru_4Al_{12}$.

Γ_8	$-0.84982| -7/2\rangle + 0.52708|5/2\rangle$
266 K	$0.52708| -5/2\rangle - 0.84982|7/2\rangle$
Γ_9	$0.94859| -9/2\rangle - 0.31473|3/2\rangle + 0.03366|15/2\rangle$
265 K	$0.03366| -15/2\rangle - 0.31473| -3/2\rangle + 0.94858|9/2\rangle$
Γ_7	$0.95955| -11/2\rangle - 0.26622|1/2\rangle + 0.09159|13/2\rangle$
212 K	$-0.09159| -13/2\rangle + 0.26622| -1/2\rangle - 0.95955|11/2\rangle$
Γ_7	$0.15592| -11/2\rangle + 0.23164|1/2\rangle - 0.96023|13/2\rangle$
125 K	$0.96023| -13/2\rangle - 0.23164| -1/2\rangle - 0.15592|11/2\rangle$
Γ_9	$-0.10171| -9/2\rangle - 0.20238|3/2\rangle + 0.97401|15/2\rangle$
118 K	$-0.97401| -15/2\rangle + 0.20238| -3/2\rangle + 0.10171|9/2\rangle$
Γ_8	$-0.52708| -7/2\rangle - 0.84982|5/2\rangle$
109 K	$0.84982| -5/2\rangle + 0.52708|7/2\rangle$
Γ_9	$0.29974| -9/2\rangle + 0.92736|3/2\rangle + 0.22399|15/2\rangle$
49 K	$0.22399| -15/2\rangle + 0.92736| -3/2\rangle + 0.29974|9/2\rangle$
Γ_7	$-0.23442| -11/2\rangle - 0.93566|1/2\rangle - 0.26378|13/2\rangle$
0 K	$-0.26378| -13/2\rangle - 0.93566| -1/2\rangle - 0.23442|11/2\rangle$

at their nonmagnetic origin. The origin of the anomalies will be discussed in Sec. IV.

IV. CEF ANALYSIS

Most of the anomalies in the magnetic and elastic properties of $Er_3Ru_4Al_{12}$ originate from CEF effects. We use the CEF model [28,29] to describe our observations. We consider the following Hamiltonian:

$$H_{\text{eff}} = H_{\text{CEF}} - \sum_i g_i O_i \varepsilon_i - \sum_i g'_i \langle O_i \rangle O_i - g_J \mu_B JH, \quad (2)$$

where the first, second, third, and fourth terms are the CEF, strain-quadrupole, quadrupole-quadrupole, and Zeeman energy, respectively. g_i is the strain-quadrupole coupling constant, O_i is the quadrupole operator, ε_i is the strain, g'_i is the quadrupole-quadrupole coupling constant, $\langle O_i \rangle$ is a thermal average of the operator O_i, $g_J = 1.2$ is the Landé factor, and $J = 15/2$ is the total angular momentum of an Er^{3+} ion. For a hexagonal symmetry, the CEF term is given by

$$H_{\text{CEF}} = B_2^0 O_2^0 + B_4^0 O_4^0 + B_6^0 O_6^0 + B_6^6 O_6^6, \quad (3)$$

where B_m^n are crystal-field parameters and O_m^n are Stevens' equivalent operators [30].

We start our analysis by calculating the matrix elements of the nonperturbed Hamiltonian, i.e., without the strain-quadrupole and quadrupole-quadrupole interactions. In this case, the eigenvectors and eigenvalues correspond to the wave functions and energies of the CEF states. Next, we included the quadrupolar interactions as a perturbation and calculated

TABLE III. CEF parameters, B_m^n (K), for $Er_3Ru_4Al_{12}$.

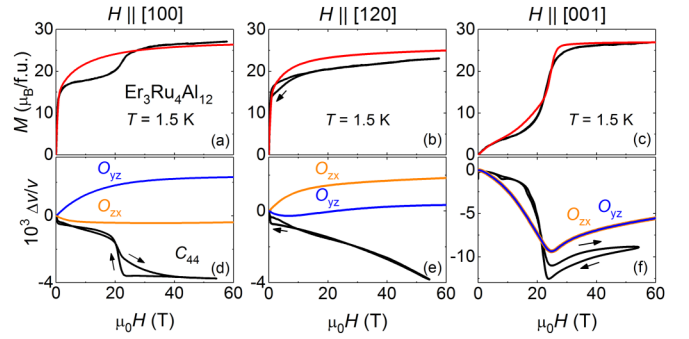| B_2^0	B_4^0	B_6^0	B_6^6
0.22(3)	$-0.0055(3)$	0.0000433(5)	$-0.00063(5)$

FIG. 5. Field dependencies of the magnetization, M, and relative sound velocity, $\Delta v/v$, for fields applied along the (a), (d) [100]; (b), (e) [120]; and (c), (f) [001] axes of $Er_3Ru_4Al_{12}$ at 1.5 K. The black curves are experimental data, the red, blue, and orange curves are the corresponding calculations within the CEF model.

the elastic modulus C_{44},

$$C_{44}(T) = C_{44}^{(0)}(T) - \frac{N_0 g^2 \chi_s(T)}{1 - g' \chi_s(T)}, \quad (4)$$

where $C_{44}^{(0)}(T)$ is the background stiffness, $N_0 = 9.525 \times 10^{27}$ m^{-3} is the number of Er ions per unit volume, and χ_s is the strain susceptibility [28]. $C_{44}^{(0)}(T)$ could be expressed as $a + bT^2 + cT^4$, where the second term is the contribution of the electronic states other than the $4f$ electrons and the third term is the phonon contribution [31]. We used $a = 76.81$ GPa, $b = -5.42 \times 10^{-5}$ GPa K^{-2}, and $c = 1.69 \times 10^{-10}$ GPa K^{-4} and approximated the relative sound-velocity changes as $\frac{\Delta v}{v} = \frac{1}{2} \frac{\Delta C}{C}$.

We also performed the CEF analysis of the magnetic susceptibility and magnetization in a similar way as done in Ref. [29]. Additional information on the CEF analysis can be found, e.g., in Refs. [15,16,20].

Based on our experimental findings and CEF analysis, we propose the following CEF scheme for $Er_3Ru_4Al_{12}$. In a hexagonal CEF, the 16-fold multiplet of the Er^{3+} ion splits in eight doublets [Fig. 4(d)]. The ground state is a Γ_7 doublet. The first excited doublet is found at 49 K, the second excited doublet at 109 K, and so on. The highest lying levels are the almost degenerate Γ_9 and Γ_8 doublets at 265 and 266 K, respectively. The wave functions of all CEF states are listed in Table II.

Using the CEF parameters listed in Table III, we can reproduce the temperature dependencies of the magnetic susceptibility [shown as $1/\chi$, Fig. 4(a)] and relative sound-velocity changes [Fig. 4(b)]. For $1/\chi$, the maximum for $H \parallel [001]$ corresponds predominantly to changes in the population of the first excited level at 49 K with temperature. For $\Delta v/v$, we obtained $|g| = 20$ K and $g' = -0.24$ K pointing to antiferroquadrupolar interactions. These values agree well with those of the isostructural $Dy_3Ru_4Al_{12}$, $Ho_3Ru_4Al_{12}$, and $U_3Ru_4Al_{12}$ compounds for which antiferroquadrupolar interactions were proposed as well [15,16,20]. The magnetic contribution to the specific heat, C_m, shows a maximum just below 40 K [Fig. 4(c)]. Qualitatively, the calculated C_m versus T dependence fits well that deduced from experimental data in Ref. [24], although the calculated values are smaller.

Our CEF analysis explains qualitatively the M versus H and $\Delta v/v$ versus H dependencies for fields applied along the [001] direction [Figs. 5(c) and 5(f)]. The jump in the magnetization and the minimum in the relative sound velocity (for both quadrupolar operators, O_{yz} and O_{zx}, for the elastic modulus C_{44} in hexagonal symmetry) around 20 T are reproduced. This proves that the anomalies observed for $H \parallel [001]$ are caused by CEF effects.

However, the CEF model cannot explain the field dependencies of the magnetization and sound velocity for $H \parallel [100]$ and $H \parallel [120]$ [Figs. 5(a), 5(b) 5(d), and 5(e)], which suggests that factors other than the CEF effects are at play. For fields applied along the [100] direction, there is no anomaly in the calculated curves [Figs. 5(a) and 5(d)]. For estimating $\Delta v/v$, we used the two quadrupolar operators, O_{yz} and O_{zx}. Although $\Delta v/v$ shows softening for O_{zx}, the overall calculated effect is much smaller than in experiment. Since the anomalies observed in experiment cannot be due to CEF transitions, one might assume that the Er magnetic moments rotate in a stepwise manner in the ordered state. However, this anomaly is also observed in the paramagnetic state, e.g., at 4.3 K [Fig. 3(d)]. Further investigations are required to address this issue. More insight into the CEF level scheme of $Er_3Ru_4Al_{12}$ can be obtained from inelastic neutron-scattering experiments (see, e.g., Refs. [32–34]).

The M versus H dependence is qualitatively reproduced for $H \parallel [120]$ [Fig. 5(b)]. However, our model predicts hardening of $\Delta v/v$ in applied field, whereas softening of $\Delta v/v$ is observed in experiment [Fig. 5(e)].

V. CONCLUSION

We studied the magnetic and elastic properties of an $Er_3Ru_4Al_{12}$ single crystal. A sharp increase in the longitudinal and transverse elastic moduli toward low temperatures below 2 K provides evidence for a phase transition at this temperature related to magnetic ordering. In the paramagnetic state, we found anomalies in the magnetization and elastic moduli as a function of temperature and magnetic field. Based on a CEF analysis that includes quadrupolar interactions, we obtain a CEF-level scheme that explains most of our observations. However, some field-induced anomalies cannot be accounted for by the CEF effects and require further studies.

[1] D. Gignoux and D. Schmitt, *Handbook of Magnetic Materials*, edited by K. H. J. Buschow (Elsevier, Amsterdam, 1997), Vol. 10.

[2] M. S. Henriques, D. I. Gorbunov, A. V. Andreev, X. Fabrèges, A. Gukasov, M. Uhlarz, V. Petříček, B. Ouladdiaf, and J. Wosnitza, Phys. Rev. B **97**, 014431 (2018).

[3] D. I. Gorbunov, M. S. Henriques, A. V. Andreev, V. Eigner, A. Gukasov, X. Fabrèges, Y. Skourski, V. Petříček, and J. Wosnitza, Phys. Rev. B **93**, 024407 (2016).

[4] T. Suzuki, T. Mizuno, K. Takezawa, S. Kamikawa, A. V. Andreev, D. I. Gorbunov, M. S. Henriques, and I. Ishii, Physica B **536**, 18 (2018).

[5] V. Chandragiri, K. K. Iyer, and E. V. Sampathkumaran, J. Phys.: Cond. Matter **28**, 286002 (2016).

[6] S. Nakamura, N. Kabeya, M. Kobayashi, K. Araki, K. Katoh, and A. Ochiai, Phys. Rev. B **98**, 054410 (2018).

[7] T. Matsumura, Y. Ozono, S. Nakamura, N. Kabeya, and A. Ochiai, J. Phys. Soc. Jpn. **88**, 023704 (2019).

[8] D. I. Gorbunov, M. S. Henriques, A. V. Andreev, Y. Skourski, and M. Dušek, J. Alloys Compd. **634**, 115 (2015).

[9] E. V. Sampathkumaran, K. K. Iyer, S. K. Upadhyay, and A. V. Andreev, Solid State Commun. **288**, 64 (2019).

[10] S. Rayaprol, A. Hoser, K. K. Iyer, S. K. Upadhyay, and E. V. Sampathkumaran, J. Magn. Magn. Mater. **477**, 83 (2019).

[11] D. I. Gorbunov, M. S. Henriques, A. V. Andreev, A. Gukasov, V. Petříček, N. V. Baranov, Y. Skourski, V. Eigner, M. Paukov, J. Prokleška, and A. P. Gonçalves, Phys. Rev. B **90**, 094405 (2014).

[12] M. S. Henriques, D. I. Gorbunov, D. Kriegner, M. Vališka, A. V. Andreev, and Z. Matěj, J. Magn. Magn. Mater. **400**, 125 (2016).

[13] V. Chandragiri, K. K. Iyer, and E. V. Sampathkumaran, Intermetallics **76**, 26 (2016).

[14] I. Ishii, K. Takezawa, H. Goto, S. Kamikawa, A. V. Andreev, D. I. Gorbunov, M. S. Henriques, and T. Suzuki, J. Phys.: Conf. Ser. **807**, 012002 (2017).

[15] I. Ishii, T. Mizuno, K. Takezawa, S. Kumano, Y. Kawamoto, T. Suzuki, D. I. Gorbunov, M. S. Henriques, and A. V. Andreev, Phys. Rev. B **97**, 235130 (2018).

[16] D. I. Gorbunov, T. Nomura, I. Ishii, M. S. Henriques, A. V. Andreev, M. Doerr, T. Stöter, T. Suzuki, S. Zherlitsyn, and J. Wosnitza, Phys. Rev. B **97**, 184412 (2018).

[17] S. Nakamura, S. Toyoshima, N. Kabeya, K. Katoh, T. Nojima, and A. Ochiai, Phys. Rev. B **91**, 214426 (2015).

[18] M. Pasturel, O. Tougait, M. Potel, T. Roisnel, K. Wochowski, H. Noël, and R. Troć, J. Phys.: Cond. Matter **21**, 125401 (2009).

[19] R. Troć, M. Pasturel, O. Tougait, A. P. Sazonov, A. Gukasov, C. Sułkowski, and H. Noël, Phys. Rev. B **85**, 064412 (2012).

[20] D. I. Gorbunov, I. Ishii, T. Nomura, M. S. Henriques, A. V. Andreev, M. Uhlarz, T. Suzuki, S. Zherlitsyn, and J. Wosnitza, Phys. Rev. B **99**, 054413 (2019).

[21] R. E. Gladyshevskii, O. R. Strusievicz, K. Cenzual, and E. Parthé, Acta Cryst. B **49**, 474 (1993).

[22] J. Niermann and W. Jeitschko, Z. Anorg. Allg. Chem. **628**, 2549 (2002).

[23] N. G. Bukhan'ko, A. I. Tursina, S. V. Malyshev, A. V. Gribanov, Y. D. Seropegin, and O. I. Bodak, J. Alloys Compd. **367**, 149 (2004).

[24] S. K. Upadhyay, K. K. Iyer, and E. V. Sampathkumaran, J. Phys.: Condens. Matter **29**, 325601 (2017).

[25] Y. Skourski, M. D. Kuz'min, K. P. Skokov, A. V. Andreev, and J. Wosnitza, Phys. Rev. B **83**, 214420 (2011).

[26] B. Lüthi, *Physical Acoustics in the Solid State* (Springer, Heidelberg, 2005).

[27] S. Zherlitsyn, S. Yasin, J. Wosnitza, A. A. Zvyagin, A. V. Andreev, and V. Tsurkan, Low Temp. Phys. **40**, 123 (2014).

[28] B. Lüthi, *Dynamical Properties of Solids*, edited by G. K. Horton and A. A. Maradudin (North-Holland, Amsterdam, 1980), Vol. 3.

[29] N. V. Hieu, T. Takeuchi, H Shishido, C. Tonohiro, T. Yamada, H. Nakashima, K. Sugiyama, R. Settai, T. D. Matsuda, Y. Haga, M. Hagiwara, K. Kindo, S. Araki, Y. Nozue, and Y. Onuki, J. Phys. Soc. Jpn. **76**, 064702 (2007).

[30] M. T. Hutchings, Solid State Phys. **16**, 227 (1964).

[31] M. Nohara, T. Suzuki, Y. Maeno, T. Fujita, I. Tanaka, and H. Kojima, Phys. Rev. B **52**, 570 (1995).

[32] O. Moze, *Handbook of Magnetic Materials*, edited by K. H. J. Buschow (Elsevier, Amsterdam, 1998), Vol. 11

[33] P. Javorský, H. Nakotte, R. A. Robinson, and T. M. Kelley, J. Magn. Magn. Mater. **186**, 373 (1998).

[34] P. Javorský, M. Diviš, H. Sugawara, H. Sato, and H. Mutka, Phys. Rev. B **65**, 014404 (2001).